On the Bandwidth of the Plenoptic Function

Minh N. Do, *Senior Member, IEEE*, Davy Marchand-Maillet, and Martin Vetterli, *Fellow, IEEE*

***Abstract*—The plenoptic function (POF) provides a powerful conceptual tool for describing a number of problems in image/video processing, vision, and graphics. For example, image-based rendering is shown as sampling and interpolation of the POF. In such applications, it is important to characterize the bandwidth of the POF. We study a simple but representative model of the scene where band-limited signals (e.g., texture images) are "painted" on smooth surfaces (e.g., of objects or walls). We show that, in general, the POF is not band limited unless the surfaces are flat. We then derive simple rules to estimate the essential bandwidth of the POF for this model. Our analysis reveals that, in addition to the maximum and minimum depths and the maximum frequency of painted signals, the bandwidth of the POF also depends on the maximum surface slope. With a unifying formalism based on multidimensional signal processing, we can verify several key results in POF processing, such as induced filtering in space and depth-corrected interpolation, and quantify the necessary sampling rates.**

***Index Terms*—Bandwidth, image-based rendering (IBR), plenoptic function (POF), sampling, spectral analysis.**

I. Introduction

EXISTING visual recording systems use a single camera and thus provide viewers with a limited and passive viewing experience. The continuing improvement in digital technology has offered low-cost sensors and massive computing power. This has led to the development of new systems employing multiple cameras together with sophisticated processing algorithms to deliver unprecedented immersive recording and viewing capabilities. Practical systems, which are called *image-based rendering* (IBR) [1], that synthesize arbitrary virtual viewpoints from several fixed sensors have already emerged; see [2]–[4] for surveys of this area.

Manuscript received December 31, 2009; revised January 07, 2010; accepted February 27, 2010. Date of publication August 08, 2011; date of current version January 18, 2012. This work was supported in part by the U.S. National Science Foundation under Grant CCF-0312432 and in part by the Swiss National Science Foundation under Grant 20-63664.00. The associate editor coordinating the review of this manuscript and approving it for publication was Prof. Hseuh-Ming Hang.

M. N. Do is with the Department of Electrical and Computer Engineering, Coordinated Science Laboratory, Beckman Institute for Advanced Science and Technology, and the Department of Bioengineering, University of Illinois at Urbana-Champaign, Urbana, IL 61801 USA (e-mail: minhdo@illinois.edu).

D. Marchand-Maillet was with the Audiovisual Communications Laboratory, École Polytechnique Fédérale de Lausanne, 1015 Lausanne, Switzerland. He is now with Energy Pool, Lyon, 69007 France.

M. Vetterli is with the Audiovisual Communications Laboratory, École Polytechnique Fédérale de Lausanne, 1015 Lausanne, Switzerland, and also with the Department of Electrical Engineering and Computer Science, University of California, Berkeley, CA 94720 USA (e-mail: martin.vetterli@epfl.ch).

Color versions of one or more of the figures in this paper are available online at http://ieeexplore.ieee.org.

Digital Object Identifier 10.1109/TIP.2011.2163895

A natural framework for studying multiview acquisition and rendering is the concept of the *plenoptic*[1] *function* (POF) [5] that describes the light intensity passing through every viewpoint, in every direction, for all time, and for every wavelength. The IBR problem can be treated as an application of the sampling theory to the POF. In this setting, acquired views from the cameras provide discrete samples of the POF, and the synthesized view is reconstructed from the continuous POF at a given point. The question of the minimum rate for sampling the POF can be addressed by spectral analysis and estimating the bandwidth of the POF.

Some of the first sampling analyses for IBR were done by Lin and Shum [6] and Chai *et al.* [7]. In particular, the work in [7] analyzes the spectral support of the POF to find an optimal uniform sampling rate for the POF. Zhang and Chen [8] extended the spectral analysis of IBR for more general cases, including non-Lambertian and occluded scenes. IBR sampling analysis has been also reviewed in detail in a recent book [4]. In these previous studies, as for any spectral-based technique, the POF is assumed to be *band limited*.

In this paper, we would like to more precisely examine the spectral analysis and band-limited assumption of the POF. To facilitate this, we study a simple but representative model where band-limited signals (e.g., texture images) are painted on smooth surfaces (e.g., of objects or walls). Using related mathematical results on domain-warped band-limited signals, we show that, in general, the POF is *not* band limited, unless the surface is flat. We then provide simple rules to estimate the essential bandwidth of the POF for this model. Unlike previous studies [6]–[8] that approximate surface by piecewise constant depth function and thus ignore the surface slope, our analysis reveals the significant role of the surface slope and is shown to provide a much more accurate estimate of the bandwidth of the POF.

It is important to note that the POF is a powerful conceptual tool for describing a number of problems in image/video processing, vision, and graphics. Most acquired and synthesized forms of visual information, including images and videos, can be treated as low-dimensional "slices" (e.g., by fixing certain variables) of the POF. Hence, the spectral analysis of the POF has applications beyond IBR. For example, see [9] for an application in light transport and [10] and [11] for applications in computational photography.

The outline of this paper is as follows: In Section II, we set up the scene and camera models and characterize the spectral support of the POF. In Section III, we start focusing on the model in which band-limited signals are "painted" on object surfaces. In Section IV, we discuss the condition for the POF to be band limited. In Section V, we derive a simple rule to estimate the essential bandwidth of time-warped functions. In Section VI,

[1] *Plenus* in Latin means complete or full.

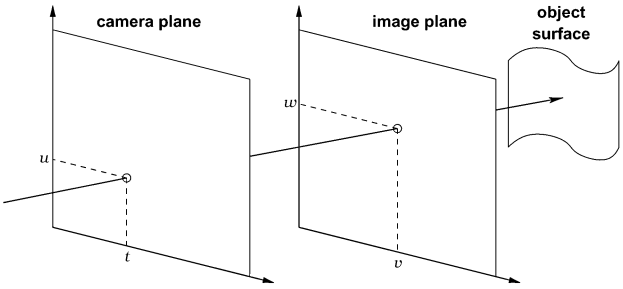

Fig. 1. Two-plane parameterization of the POF. Each light ray is specified by a 4-D coordinate (t, u, v, w), where (t, u) corresponds to the camera location in the *camera plane* and (v, w) corresponds to the image point (or pixel) in the *image plane*. Effectively, (t, u) specifies the viewing position, and (u, w) specifies the viewing angle.

we apply this rule to derive estimates the essential bandwidths of the POF and illustrate with an example where the proposed method provides much more accurate estimates, compared with previous studies. In Section VII, we show that multidimensional spectral analysis of the sheared POF leads to a new interpretation of the effectiveness of depth-corrected interpolation in IBR. Some preliminary results of this paper were presented at a conference [12].

II. Scene and Camera Models

A convenient way to parameterize the POF is to use the two-plane parameterization, also known as light field or lumigraph [13], [14], as shown in Fig. 1. By restricting the scene in a bounding box, each light ray can be specified by a pair of coordinates (t, u) and (v, w) corresponding to the locations of the camera and the image pixel within a camera, respectively. Note that image coordinate (v, w) is relatively defined with respect to camera position (t, u). Hence, equivalently, (t, u) specifies the viewing position, and (u, w) specifies the viewing angle.

The two-plane parameterization fits the *pinhole* camera model [15], in which all pixels in a camera correspond to light rays that are emitted from one point—the camera position. The value of POF $p(t, u, v, w)$ is the light intensity captured by a camera at location (t, v) and at pixel location (v, w) within that camera. In general, $p(t, u, v, w)$ is the light intensity at the intersection of the ray specified by (t, u, v, w) with the nearest object surface to camera position (t, v).

For simplicity of exposition, and as in [7] and [8], we consider a 2-D version of the POF, i.e., $p(t, v)$, by fixing u and w. This corresponds to the situation where the cameras are placed on a straight line, and we consider the same image scan line from each camera. Alternatively, we could view this as a flatland model where the 3-D world is "flattened" into a 2-D plane. Function $p(t, v)$ is also known as epipolar-plane image (EPI) [16] and plays an important role in computer vision [15], [17].

We consider the scene model, as shown in Fig. 2, that consists of an object surface (in the 2-D setting of the POF, this is a slice of the surface) specified by its varying depth $z(t)$. Without loss of generality, we rescale depth value z so that the focal length or distance between the camera and image planes is equal to 1. This scene model represents a *microscale analysis* of the POF, where, locally, only one object surface is visible.

Suppose that light ray (t, v) specified by camera (or viewing) position t and pixel position (or viewing angle) v intersects with the object surface at a point with coordinate $(x, z(x))$, as shown in Fig. 2. Then, simple geometric relations lead to

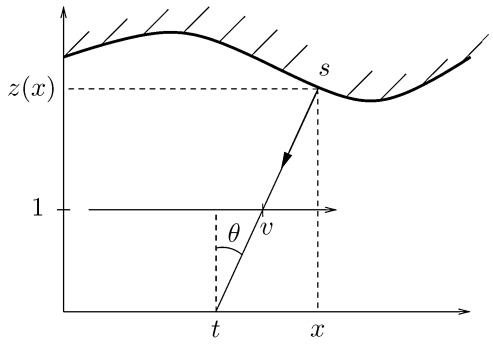

Fig. 2. Scene model with functional surface $z(x)$. Coordinates t, v, and z specify the camera position, pixel position, and depth, respectively. The depth axis is rescaled so that the focal length or the distance between t and v axes is 1, and thus, pixel position v is related to viewing angle θ by $v = \tan(\theta)$.

$$t = x - z(x)\ \tan(\theta) = x - z(x)v. \tag{1}$$

Equation (1) defines a fundamental *geometric mapping* that links light ray (t, v) to position s specified by x on the object surface that is "seen" by this light ray.

We assume that there is *no self-occlusion* on the object surface in the field-of-view of the cameras. This means that each light ray (t, v) within the field-of-view can intersect with at most one point on object surface $z(x)$. This is equivalent to requiring that t given in (1) is a strictly monotonic function of x, which amounts to

$$|z'(x)| < \frac{1}{v_{\max}} \tag{2}$$

where the field-of-view is limited by $|v| \leq v_{\max}$. In other words, the slope of object surface $z(x)$ is bounded by the maximum viewing angle. For POF spectral analysis and IBR sampling analysis methods that consider occluded scenes, we refer readers to [8] and [18].

Let $l(x, v)$ be the light intensity emitted from object surface position x and viewing angle v (see Fig. 2). Function $l(x, v)$ is also known as the *surface light field* [19] or *surface POF* [8]. Then, using (1) and under the no self-occlusion assumption, we have

$$p(t, v) = l(x, v), \quad \text{where} \quad t = x - z(x)v. \tag{3}$$

Taking the Fourier transform of POF $p(t, v)$ using (3), we obtain

$$\begin{aligned} P(\omega_t, \omega_v) &\stackrel{\text{def}}{=} \mathcal{F}_{t,v}\left\{p(t, v)\right\} \\ &= \int_{-\infty}^{\infty}\int_{-\infty}^{\infty} p(t, v)\, e^{-j(\omega_t t + \omega_v v)}\, dtdv \\ &= \int_{-\infty}^{\infty}\int_{-\infty}^{\infty} l(x, v)\, e^{-j(\omega_t(x - z(x)v) + \omega_v v)}\ (1 - z'(x)v)\ dxdv \\ &= \int_{-\infty}^{\infty} e^{-j\omega_t x} \int_{-\infty}^{\infty} (1 - z'(x)v)\ l(x, v)\, e^{-j(\omega_v - z(x)\omega_t)v}\, dvdx \end{aligned}$$

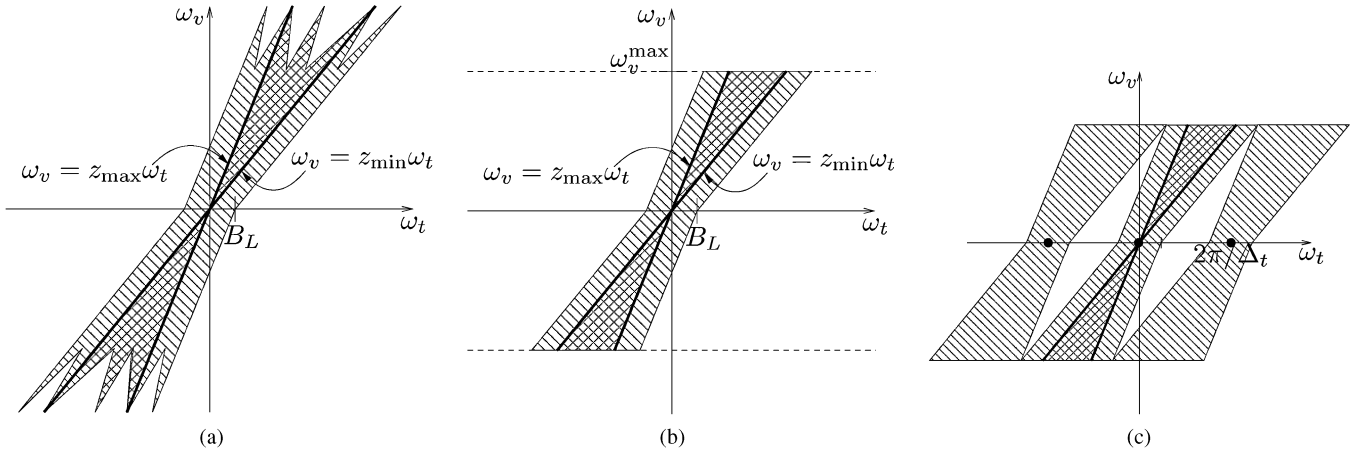

Fig. 3. Spectral supports of POF $p(t, v)$. (a) The original support is contained between two lines corresponding to the minimum and maximum depths, plus an extended region accounting for non-Lambertian surfaces. (b) Low-pass filtering in pixel dimension v induces low-pass filtering in spatial dimension t. (c) Sampling in space along t leads to periodization in frequency along ω_t.

$$= \int_{-\infty}^{\infty} e^{-j\omega_t x}\, H\left(x, \omega_v - z(x)\omega_t\right)\, dx \tag{4}$$

where we denote $h(x,v) \stackrel{\text{def}}{=} (1 - z'(x)v)\ l(x,v)$ and $H(x,\omega_v) \stackrel{\text{def}}{=} \mathcal{F}_v\{h(x,v)\} = \int_{-\infty}^{\infty} h(x,v)\ e^{-j\omega_v v}\ \mathrm{d}v$. Similarly, we denote $L(x,\omega_v) \stackrel{\text{def}}{=} \mathcal{F}_v\{l(x,v)\}$, and then Fourier transform properties lead to

$$H(x,\omega_v) = L(x,\omega_v) - jz'(x)\frac{\partial L(x,\omega_v)}{\partial \omega_v}. \tag{5}$$

Typically, except for rare cases of highly specular surfaces, at fixed surface position x, emitted light intensity $l(x,v)$ very slowly changes with respect to viewing angle v. In the extreme case, the surface is often assumed to be *Lambertian* [17], which means $l(x,v) = l(x)$ for all v. Thus, it is reasonable to assume that $l(x,v)$ is a band-limited function in variable v. Using (4) and (5), we immediately obtain the following result.

Proposition 1: Given the no-self-occlusion condition (2) and suppose that

$$L(x,\omega_v) = 0, \quad \text{if} |\omega_v| > B_L \tag{6}$$

then

$$P(\omega_t,\omega_v) = 0, \quad \text{if } |\omega_v - z(x)\omega_t| > B_L \text{ for all } x. \tag{7}$$

Therefore, as shown in Fig. 3(a), the spectral support of POF $p(t,v)$ is contained between two lines corresponding to minimum and maximum depths, plus an extended region accounting for non-Lambertian surfaces. This key finding was first discovered by Chai *et al.* [7] for Lambertian surfaces and later extended by Zhang and Chen [8] for non-Lambertian surfaces. However, in both of these previous studies, the derivations are approximations based on "truncating windows," in which the scene is approximated by piecewise constant depth segments, and the truncation effect in the spectral domain is ignored. Here, we show that for no-self-occlusion surfaces with band-limited light radiance, the resulting POF has spectral support *exactly* contained in the region specified by (7).

This "bow-tie" shape spectral support of POF $p(t,v)$ makes it possible to induce *continuous-domain* low-pass filtering in spatial dimension t via *induced filtering* in pixel dimension v. Generally, it is physically impossible to realize continuous-domain filtering in the spatial dimension since we do *not* have access to the POF in the continuous domain of t but rather only at discrete locations where we have actual cameras. On the other hand, continuous-domain low-pass filtering in pixel dimension v is possible by the optical system in the cameras. Because of the "bow-tie" shape spectral support of the POF, Fig. 3(b) illustrates that low-pass filtering in v induces low-pass filtering in t as well. As a result, Fig. 3(c) shows that we can sample the POF in space (i.e., by placing cameras at discrete location along t) without alias. This induced filtering property also holds for sound signals, as was shown in a study of the *plenacoustic* function [20].

Typically, POF $p(t,v)$ is captured by cameras with *finite pixel resolution* Δ_v along pixel dimension v. Thus, previous analyses [7], [8] *assume* that $P(\omega_t,\omega_v)$ is band limited in the ω_v dimension to $|\omega_v| \le \pi/\Delta_v$. Based on this assumption and using Proposition 1 and Fig. 3(b), it follows that the bandwidth of the POF depends only on the range of depths and the pixel resolution.

However, actual continuous-domain POF $p(t,v)$ might *not* be band limited according to the camera resolution. In some applications, it might be of interest to study the intrinsic bandwidth of the POF according to the underlying scene rather than the capturing devices. In this paper, we want to characterize the bandwidth of POF $p(t,v)$ according to a simple but representative scene model that will be described in the next section.

III. Surface Model: Signals Painted on Surfaces

First, we restrict to Lambertian surfaces, i.e., $l(x,v) = l(x)$. Second, we assume that light radiance $l(x)$ is a result of band-limited signal $f(s)$ (e.g., texture image) "painted" on the object surface, where $s = s(x)$ is the curvilinear coordinate (i.e., s corresponds to the arc length) on the surface. That is

$$l(x) = f\left(s(x)\right).$$

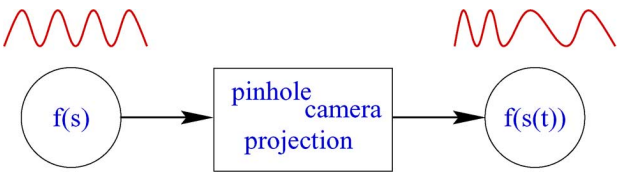

Fig. 4. Mapping from $f(t)$ to $(f \circ s)(t) = f(s(t))$ due to the pinhole camera projection.

Surface coordinate x is determined by light ray coordinate (t, v) as $x = x(t, v)$ according to the geometric mapping equation (1) as

$$t = x(t, v) - v\, z\left(x(t, v)\right). \tag{8}$$

With a slight abuse of notation, we write $s(t, v) = s(x(t, v))$ for the composite mapping from light ray coordinate (t, v) to curvilinear coordinate s on the surface. With these mappings, we can relate POF $p(t, v)$ to "painted" signal $f(s)$ on the object surface as

$$p(t, v) = l\left(x(t, v)\right) = f\left(s\left(x(t, v)\right)\right) = f\left(s(t, v)\right). \tag{9}$$

We study the bandwidth of POF $p(t, v)$ by fixing either t or v. Note that fixing t in POF $p(t, v)$ corresponds to considering an image captured by a fixed camera, whereas fixing v corresponds to considering a signal recorded at a fixed pixel location by a moving camera. In both cases, we obtain a *time-warped* function of band-limited function $f(s(t))$, where t and s denote a generic variable and warping function, respectively. Fig. 4 depicts this generic case study of the POF.

Fixing either v or t and taking the derivative of (8) with respect to the other variable, we get

$$\frac{\partial x(t, v)}{\partial t} = \frac{1}{1 - v\, z'(x)} \tag{10}$$

$$\frac{\partial x(t, v)}{\partial v} = \frac{z(x)}{1 - v\, z'(x)}. \tag{11}$$

Hereafter, for brevity, in the right-hand sides, we write x for $x(t, v)$. The no-self-occlusion condition (2) implies that both of these partial derivatives are positive for $v \in [-v_{\max}, v_{\max}]$ or within the field-of-view. This means that $x(t, v)$ is a strictly monotonic function in each coordinate t and v. Using differential relation $ds = \sqrt{dx^2 + dz^2} = \sqrt{1 + (z'(x))^2}dx$, we obtain the partial derivatives of s with respect to t and v as

$$\frac{\partial s(t, v)}{\partial t} = \frac{ds}{dx}\frac{\partial x(t, v)}{\partial t} = \frac{\sqrt{1 + \left(z'(x)\right)^2}}{1 - v\, z'(x)} \tag{12}$$

$$\frac{\partial s(t, v)}{\partial v} = \frac{ds}{dx}\frac{\partial x(t, v)}{\partial v} = \frac{z(x)\sqrt{1 + \left(z'(x)\right)^2}}{1 - v\, z'(x)}. \tag{13}$$

From (12), we see that if the surface is flat, i.e., $z'(x)$ is a constant, then $\partial s(t, v)/\partial t$ is a constant, or $s(t, v)$ is a linear function in t for each fixed v. Conversely, under the no-self-occlusion condition (2), if $s(t, v)$ is linear for fixed v, then it is easy to see that $z'(x)$ must be a constant, and thus, the surface must be flat.

Finally, we note that both partial derivatives of s given in (12) and (13) are greater than 1.

IV. Band-limited POFs

As noted in the introduction, to address the sampling problem of the POF, we need to study its spectral support. Here, we examine the band limitedness of the POF given in (9). In plenoptic sampling for IBR, the main variable of interest is t, which is the camera position, as it leads to conditions on how to place the cameras. Thus, let us consider the situation where pixel position v is fixed, and for brevity, we drop variable v in functions in this section.

Again, suppose that painted signal $f(s)$ is band limited. From the discussion at the end of the last section, we note that if the surface in our scene is flat, then $s(t)$ is linear and POF $p(t) = f(s(t))$ is a uniformly stretched version of $f(t)$. Thus, it immediately follows from the shifting and scaling properties of Fourier transform that $f(s(t))$ is also band limited. We are interested to know if there are any other surfaces that result in band-limited POFs.

Time-warped band-limited functions have been studied in the signal processing literature. In [21], Clark conjectured that when band-limited function f is warped by monotonic function s, the resulting function $(f \circ s)(t) = f(s(t))$ is also band limited *if* and *only if* $s(t)$ is linear. In [22], this conjecture was proved for a large class of $s(t)$, in particular, for $s(t)$ that on certain interval is a restriction of an entire function.[2] Later, in [23], Clark's conjecture was shown to be false by a peculiar counterexample constructed by Y. Meyer. However, that paper also noted that it is not possible for a nonlinear warping function to preserve band limitedness in general. Unaware of this line of work, in [24], we made the same conjecture on the preservation of band limitedness under warping.

The implication of the above result is that, in general, the POF is *not* band limited unless the surface is flat. In the next sections, we will study the *essential bandwidth*, defined as the bandwidth where most of the signal energy resides, of the POF for general smooth surfaces.

V. Bandwidth of Time-Warped Functions

Let $g(t) = (f \circ s)(t)$ denote a time-warped function that models the POF, as was described in Section III. Its Fourier transform is

$$G(\omega_t) = \int_{-\infty}^{\infty} f\left(s(t)\right) e^{-j\omega_t t} \mathrm{d}t. \tag{14}$$

Let $F(\omega_s)$ be the Fourier transform of $f(s)$. Then

$$f(s) = \frac{1}{2\pi}\int_{-\infty}^{\infty} F(\omega_s) e^{j\omega_s s} \mathrm{d}\omega_s. \tag{15}$$

[2]An entire function is a function of complex variable that has derivative at each point in the entire finite plane. In particular, band-limited functions are entire functions.

Substituting (15) into (14), we obtain

$$G(\omega_t) = \frac{1}{2\pi}\int_{-\infty}^{\infty} F(\omega_s)\left(\int e^{j\omega_s s(t)}e^{-j\omega_t t}\mathrm{d}t\right)\mathrm{d}\omega_s$$
$$= \frac{1}{2\pi}\int_{-\infty}^{\infty} F(\omega_s)K_s(\omega_t,\omega_s)\mathrm{d}\omega_s \quad (16)$$

where $K_s(\omega_t,\omega) \stackrel{\text{def}}{=} \mathcal{F}_t\{e^{j\omega_s s(t)}\}$ is the Fourier transform of $e^{j\omega_s s(t)}$. Kernel function $K_s(\omega_t,\omega_s)$ characterizes how warping function s broadens the spectrum of f in warped function $g = f\circ s$. To see this effect, first consider the case when s is a linear function, i.e., $s(t) = a + bt$. In this case, we have

$$K_s(\omega_t,\omega_s) = \mathcal{F}_t\left\{e^{j\omega_s(a+bt)}\right\} = 2\pi e^{ja\omega_s}\delta(\omega_t - b\omega_s) \quad (17)$$

which is concentrated along line $\omega_s = \omega_t/b$. Substituting (17) into (16), we get

$$G(\omega_t) = \frac{e^{ja\omega_t/b}}{|b|}F\left(\frac{\omega_t}{b}\right).$$

Thus, for linear warping $s(t) = a + bt$, we can relate the bandwidth of warped function $g = f\circ s$ to the bandwidth of f as

$$\mathrm{BW}\{g\} = |b|\,\mathrm{BW}\{f\} = |s'|\,\mathrm{BW}\{f\}. \quad (18)$$

Next, consider a more general situation in which warping function s deviates from a linear function as

$$s(t) = a + bt + \tilde{s}(t). \quad (19)$$

Then, kernel $K_s(\omega_t,\omega_s)$ becomes

$$K_s(\omega_t,\omega_s) = \mathcal{F}_t\left\{e^{j\omega_s(a+bt)}\cdot e^{j\omega_s\tilde{s}(t)}\right\}$$
$$= 2\pi e^{ja\omega_s}\delta(\omega_t - b\omega_s) *_{\omega_t} \mathcal{F}_t\left\{e^{j\omega_s\tilde{s}(t)}\right\} \quad (20)$$

where $*_{\omega_t}$ denotes the convolution in variable ω_t.

Consider a simple case where deviation $\tilde{s}(t)$ is an oscillation function with single frequency $\mu > 0$, i.e., $\tilde{s}(t) = c\sin(\mu t)$. Using the following expansion:

$$e^{jx\sin(\alpha)} = \sum_{n=-\infty}^{\infty} J_n(x)e^{jn\alpha}$$

where $J_n(x)$ is the nth-order Bessel function of the first kind, we have

$$\mathcal{F}_t\left\{e^{j\omega_s c\sin(\mu t)}\right\} = 2\pi\sum_{n=-\infty}^{\infty} J_n(c\omega)\,\delta(\omega_t - n\mu).$$

Bessel functions $J_n(x)$ exponentially decay for sufficiently large n and are negligible for $|n| > |x| + 1$. Thus, for $\tilde{s}(t) = c\sin(\mu t)$, Fourier transform $\mathcal{F}_t\{e^{j\omega_s\tilde{s}(t)}\}$ is essentially zero for frequency $|\omega_t| > |c\mu\omega_s| + \mu$. Based on this approximation, substituting back in (20) and then (16), we see that the *essential bandwidth* of g is

$$\mathrm{essBW}\{g\} = (|b| + |c\mu|)\ \mathrm{BW}\{f\} + \mu. \quad (21)$$

Note that in this case $s(t) = a + bt + c\sin(\mu t)$, we can write $|b| + |c\mu| = \max|s'|$. Moreover, for the POF, typically, the oscillation of surface s is much smaller than the oscillation of painted texture f; therefore, $\mu \ll \mathrm{BW}\{f\}$. Furthermore, as noted at the end of Section III, for POF, $|s'| > 1$. Thus, from (21), we can write

$$\mathrm{essBW}\{g\} = (\max|s'|)\ \mathrm{BW}\{f\}. \quad (22)$$

In words, the essential bandwidth of time-warped function $g(t) = f(s(t))$ can be approximated by the product of the maximum derivative of s with the bandwidth of f.

Rule (22) can be approximated for general warping function s as follows. Since, typically, s is smooth, it can be approximated by a piecewise linear function, i.e.,

$$\hat{s}(t) \stackrel{\text{def}}{=} s(t_k) + s'(\xi_k)(t - t_k) \quad \text{for } t\in[t_k, t_{k+1}] \quad (23)$$

with appropriately chosen $\xi_k \in [t_k, t_{k+1}]$ and sufficiently small segments $[t_k, t_{k+1}]$. Then, time-warped function $g(t) = f(s(t))$ can be approximated by

$$\hat{g}(t) \stackrel{\text{def}}{=} f\left(\hat{s}(t)\right)$$
$$= f\left(s(t_k) + s'(\xi_k)(t - t_k)\right) \quad \text{for } t\in[t_k, t_{k+1})$$
$$= \sum_k f\left(s(t_k) + s'(\xi_k)(t - t_k)\right)\ b_k(t) \quad (24)$$

where $b_k(t)$ is the indicator function of interval $[t_k, t_{k+1}]$, i.e., $b_k(t)$ is equal to 1 for $t \in [t_k, t_{k+1}]$ and 0 otherwise. Denote $f_k(t) = f(s(t_k) + s'(\xi_k)(t - t_k))$, which is a linear warping. Then, we can relate the bandwidth of f_k to the bandwidth of f as

$$\mathrm{BW}\{f_k\} = |s'(\xi_k)|\ \mathrm{BW}\{f\}.$$

Since $b_k(t)$ is a rectangular function of length $(t_{k+1} - t_k)$, its Fourier transform $B_k(\omega)$ is a *sinc* function with the following essential bandwidth:

$$\mathrm{essBW}\{b_k\} = \frac{1}{t_{k+1} - t_k}.$$

From (24), it follows that $\widehat{G}(\omega) = \sum_k F_k(\omega) * B_k(\omega)$, and hence:

$$\mathrm{essBW}\{\hat{g}\} = \max_k\left(|s'(\xi_k)|\ \mathrm{BW}\{f\} + \frac{1}{t_{k+1} - t_k}\right). \quad (25)$$

For the POF, typically, the oscillation of s is much smaller than the oscillation of f. Therefore, a good approximation of $f(s(t))$ can be obtained from $f(\hat{s}(t))$ using a piecewise linear approximation of $s(t)$, as in (23), with $\max_k 1/(t_{k+1} - t_k) \ll \mathrm{BW}\{f\}$. Thus, we can discard the second term on the right-hand side of (25) and obtain

$$\mathrm{essBW}\{g\} \approx \mathrm{essBW}\{\hat{g}\} \approx (\max|s'|)\ \mathrm{BW}\{f\}. \quad (26)$$

Note that this approximation is exact for linear warping s, as shown in (18).

The bandwidth analysis of time-warped functions in this section follows the bandwidth analysis of frequency-modulation

signals in communication systems [25]. A similar rule like (26) is called Carson's rule in the communication systems literature. We note that both Carson's rule and (26) are difficult to precisely prove, except for some particular cases, and thus, they should only be viewed as "rules of thumb." In the next sections, we will show that rule (26) is quite accurate and provides an effective mean to estimate the bandwidth of the POFs.

VI. Bandwidth of the POFs

The result from the last section reveals the role of the maximum absolute value of the derivatives of curvilinear coordinate s on the bandwidth of the POF. These maximum derivatives represent the *worst cases* of the multiplicative term in the bandwidth expansion of the POF, as given in (26).

More precisely, denote again BW_f the bandwidth of "painted" signal f on the object surface. Then, applying (12) and (13) to rule (26), we obtain the following estimates of the essential bandwidth of POF $p(t,v)$ in dimensions t and v, denoted by $\mathrm{essBW}_t\{p\}$ and $\mathrm{essBW}_v\{p\}$, respectively:

$$\begin{aligned}\mathrm{essBW}_t\{p\} &= \left(\max\frac{\partial s(t,v)}{\partial t}\right)\mathrm{BW}\{f\}\\ &= \frac{\sqrt{1+\max|z'|^2}}{1-v_{\max}\max|z'|}\,\mathrm{BW}\{f\} \qquad (27)\\ \mathrm{essBW}_v\{p\} &= \left(\max\frac{\partial s(t,v)}{\partial v}\right)\mathrm{BW}\{f\}\\ &\le \frac{z_{\max}\sqrt{1+\max|z'|^2}}{1-v_{\max}\max|z'|}\,\mathrm{BW}\{f\}. \qquad (28)\end{aligned}$$

The above results (27) and (28) imply that when varying camera position t, the worst case of bandwidth expansion for the POF comes from the steepest slope (with respect to the camera axis) on the object surface. When varying pixel position v, the worst case happens when the surface is at the steepest point and furthest, and the pixel is at the boundary of the field-of-view. These findings are also noted in the literature on texture mapping and image warping [26].

Note that (27) is an equality, whereas (28) is an inequality because $|z(x)|$ and $|z'(x)|$ might not be maximum at the same x. One way to characterize the spectral support of the POF is to use (27) to estimate the spectral support along the t dimension and then use Proposition 1 to estimate the multidimensional spectrum support in the joint t–v space.

Recall that previous POF spectral analyses [7], [8] were based on piecewise constant depth approximation. In formulations (27) and (28), this means assuming that $z'(x)=0$, and thus, $\mathrm{essBW}_t\{p\}=\mathrm{BW}\{f\}$. Consequently, previous studies show that the multidimensional spectral support of the POF depends only on the bandwidth of the painted texture and the minimum and maximum depths. Our analysis reveals that, in addition, surface slope $z'(x)$ also influences the bandwidth of the POF, namely, bigger surface slope leads to larger POF bandwidth. Estimates (27) and (28) precisely quantify this influence.

To illustrate and validate these rules for estimating the bandwidth of the POF, we consider a synthetic scene, as shown in Fig. 5. Note that, as before, all length measures are normalized so that the focal length (i.e., the distance between t and v axes) is equal to 1. In the scene, there is a *curved wall* as an arc of a circle with radius R and center at distance C from the origin on the z-axis. Texture signal $f(s)=\sin(2\pi\kappa s)$ of frequency κ is painted on the wall. For convenience, we also specify a point on the object surface by angle α between the corresponding radial line with the z-axis (see Fig. 5). Then

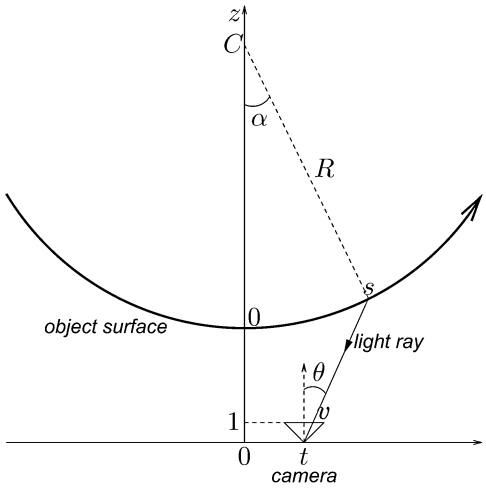

Fig. 5. Scene with a curved wall that is used in numerical experiments.

$$\begin{cases}\frac{x}{R}=\sin(\alpha)\\ \frac{C-z(x)}{R}=\cos(\alpha)\\ s=\alpha R.\end{cases}$$

It follows that:

$$z'(x)=\tan(\alpha).$$

Substituting (29) into the geometric mapping equation (1) and using θ to specify the pixel position, i.e., $v=\tan(\theta)$, we get

$$t=R\sin(\alpha)-(C-R\cos(\alpha))\tan(\theta).$$

From this, we can express curvilinear coordinate s on the object surface through light ray coordinates (t,v) as [noting $\theta=\tan^{-1}(v)$]

$$s=R\left(\sin^{-1}\left(\frac{t\cos(\theta)+C\sin(\theta)}{R}\right)-\theta\right). \qquad (30)$$

Fig. 6(b) shows the resulting POF of a curved wall with $C=20$, $R=10$, and $\kappa=2$. The examined ranges of t and v are $t\in[-3,+3]$ and $v\in[-0.35,+0.35]$ (with the focal length normalized to 1, this is equivalent to using 50-mm lens on a 35-mm camera). With these parameters, the surface depth is in range $z(x)\in[10,13.76]$ and the surface slope is in range $z'(x)\in[-1.25,1.25]$. Plugging these values into (27) and (28), we obtain the following estimates for the essential maximum frequencies of $P(\omega_t,\omega_v)$ as:

$$\begin{cases}\omega_t^{\max}/(2\pi)=5.7Hz,\\ \omega_v^{\max}/(2\pi)=78.6Hz.\end{cases}$$

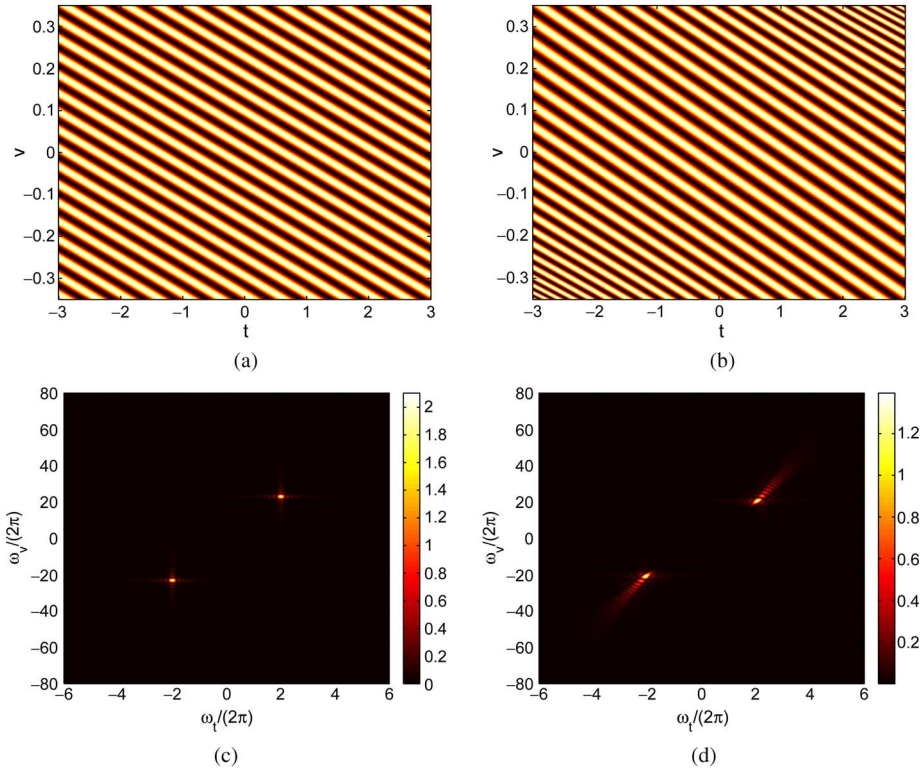

Fig. 6. Examples of POF $p(t, v)$ and its Fourier transform $P(\omega_t, \omega_v)$ for flat and curved walls. (a) Flat wall: $p(t, v)$. (b) Curved wall: $p(t, v)$. (c) Flat wall: $P(\omega_t, \omega_v)$. (d) Curved wall: $P(\omega_t, \omega_v)$.

These estimates agree well with the plot of $P(\omega_t, \omega_v)$ for the curved wall in Fig. 6(d). Additionally, note in the plot that the spectral support of the POF is sandwiched between lines $\omega_v = z_{\min}\omega_t$ and $\omega_v = z_{\max}\omega_t$, as illustrated in Fig. 3.

For comparison, Fig. 6(a) and (c) show the POF and its spectrum for the same camera configuration and painted texture, except that the wall is *flat* at constant depth $z(x) = 11.5$. Compared with the *flat-wall* case, the spectrum support of the POF of the curved wall is significantly broader, both in the angle and the radial length of the cone-shape region illustrated in Fig. 3. The angular broadening of the POF spectrum is due to the varying of surface depth $z(x)$, as was previously noted in [7]. However, the radial broadening of the POF spectrum, which is due to maximum surface slope $z'(x)$, as indicated in (27) and (28), is only revealed in this paper.

VII. Bandwidth of Sheared POFs

The results in the last section characterize the bandwidths of POF $p(t, v)$ in each dimension t and v *separately*. For plenoptic sampling, such bandwidths are relevant if we sample and reconstruct along each dimension t and v separately while fixing the other dimension. However, the typical shapes of POF spectral supports, as shown in Figs. 3 and 6(c) and (d), indicate that we can compact the POF spectrum more (and hence have less aliasing in sampling) by *nonseparably* processing the two dimensions t and v. In particular, using the knowledge of minimum and maximum depths, i.e., $z_{\min}$ and $z_{\max}$, and the property of POF spectral support, as shown in Fig. 3, optimal *nonseparable* reconstruction filters for IBR were derived in [7] and [8].

An alternative approach to explore this property of the POF spectrum support in IBR using only 1-D reconstruction filter is as follows. Since the POF spectral support is slanted according to the depth range, *shearing* the POF spectrum, as shown in Fig. 7(c) and (d), would make it more compact along the ω_t axis. Fig. 7(a) and (b) illustrate the spatial supports of the corresponding functions with the spectra given in Fig. 7(c) and (d), namely, the POF and its sheared version. More precisely, the desired shearing operator is obtained by the following change of variable in the frequency domain:

$$\begin{cases} \omega_{t'} = \omega_t - \omega_v/z_0, \\ \omega_{v'} = \omega_v. \end{cases}$$

The corresponding change of variable in the space domain is

$$\begin{cases} t' = t, \\ v' = v + t/z_0. \end{cases}$$

Geometrically, this shearing operator maps, in the frequency domain, line $\omega_v = z_0\omega_t$ into the $\omega_{v'}$ axis [i.e., from Fig. 7(c) and (d)], or equivalently, in the space domain, it maps the t axis into line $v' = t'/z_0$ [i.e., from Fig. 7(a) and (b)]. Therefore, with a suitable choice of z_0 such that $z_{\min} \le z_0 \le z_{\max}$, the spectrum of sheared POF is more compact along the $\omega_{t'}$ axis. Optimal depth z_0 suggested in [7] satisfies

$$\frac{1}{z_0} = \frac{1}{2}\left(\frac{1}{z_{\min}} + \frac{1}{z_{\max}}\right)$$

which can be obtained through Fig. 3.

With the compact spectrum along the $w_{t'}$ axis, we can achieve high-quality reconstruction (i.e., less aliasing) for the sheared

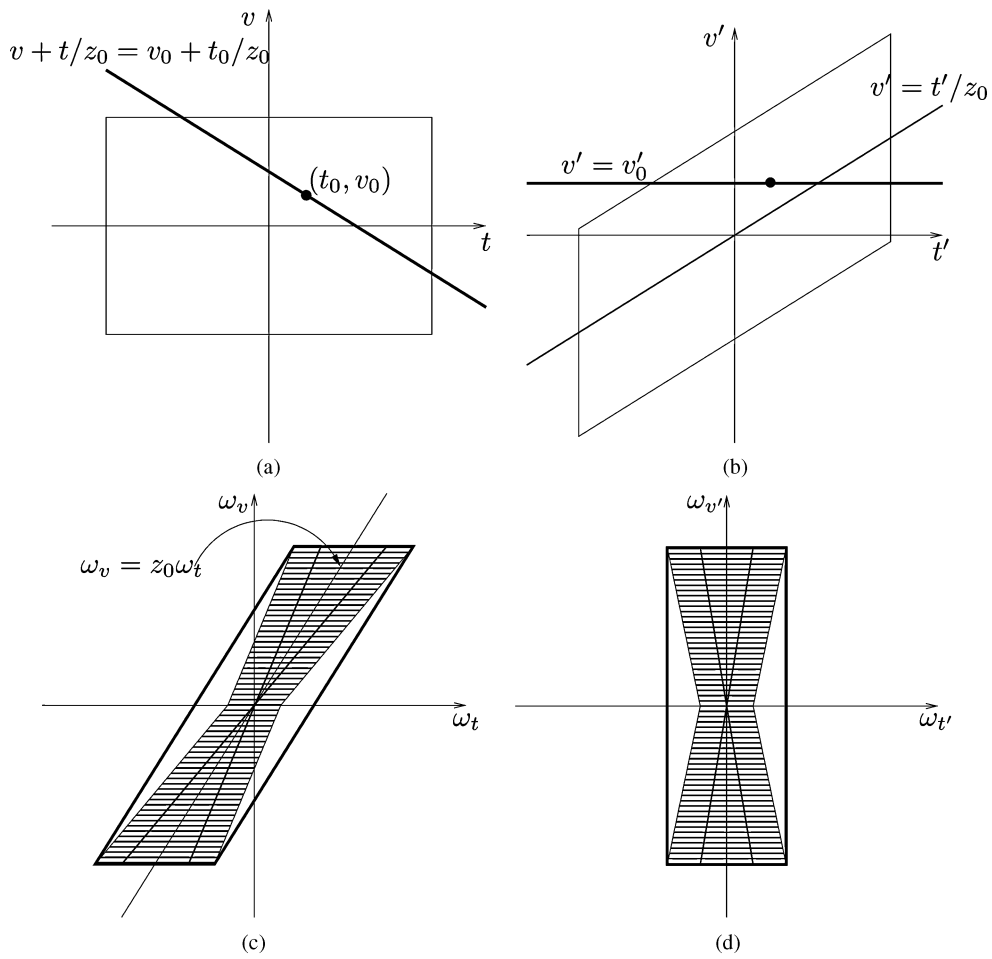

Fig. 7. Sheared spectrum of the POF by a change of variable, i.e., $\omega_{t'} = \omega_t - (1/z_0)\omega_v$ and $\omega'_v = \omega_v$. With appropriate choice of z_0, the sheared spectrum is most compacted near the ω'_v axis. (a) The POF. (b) The sheared POF. (c) Spectrum of the POF. (d) Spectrum of the sheared POF.

POF by simply reconstructing along t' axis for each fixed v'. In other words, we interpolate the sheared POF along lines $v' = v'_0$. It is easy to see that corresponding to line $v' = v'_0$ in the sheared domain is the following line in the original domain [see Fig. 7(a) and (b)]:

$$v + t/z_0 = v_0 + t_0/z_0. \tag{31}$$

Therefore, equivalently, we can obtain high-quality reconstruction of the original POF $p(t, v)$ at location (t_0, v_0) by interpolating along line (31). From (1), we see that all corresponding light rays (t, v) that satisfy line (31) intersect with light ray (t_0, v_0) at the same point of depth z_0.

The lumigraph [14] system employs the same reconstruction strategy, which they call *depth-corrected* interpolation. Gortler *et al.* [14] refer to line (31) as an *optical low* line (where the object surface "seen" by the light ray (t_0, v_0) is assumed to be at depth z_0), and they expect the POF to be smooth along the optical flow lines. Their experiments show that reconstruction by depth-corrected interpolation along the optical flow lines has significantly higher quality compared with uncorrected interpolation (i.e., interpolate along same pixel lines $v = v_0$).

We can characterize the smoothness of the POF along optical flow line (31) by estimating the bandwidth of the 1-D slice function of the POF along this line (which is also the 1-D function along line $v' = v'_0$ of the sheared POF). The corresponding derivative for the bandwidth expanding factor in (22) is the *directional derivative* of s along line (31), with unit vector $\boldsymbol{u} = (1, -1/z_0)$. Using (12) and (13), we obtain the derivative of s in this direction as

$$\begin{aligned} D_{\boldsymbol{u}} s(t, v) &= \boldsymbol{u}_t \frac{\partial s(t, v)}{\partial t} + \boldsymbol{u}_v \frac{\partial s(t, v)}{\partial v} \\ &= \frac{(1 - z(x)/z_0)\sqrt{1 + (z'(x))^2}}{1 - v\, z'(x)}. \end{aligned} \tag{32}$$

Comparing $D_{\boldsymbol{u}} s$ in (32) to $\partial s/\partial t$ in (12), we see that, with a suitable choice of z_0 such as $z_0 = (z_{\min} + z_{\max})/2$, the absolute value of the derivative of s in direction $\boldsymbol{u} = (1, -1/z_0)$ is smaller than the one in direction (1, 0). Hence, according to (22), the bandwidth of the POF along optical flow line (31) is smaller than the bandwidth along the same pixel line $v = v_0$.

Fig. 8 shows example slices of the POF for the *curved-wall* scene described in Section VI along the same pixel line $v = v_0$ and optical flow line (31) with $t_0 = v_0 = 0$ and $z_0 = 11.5$. We see that the maximum frequency of the POF slice along the optical flow is much smaller compared with the one along the same

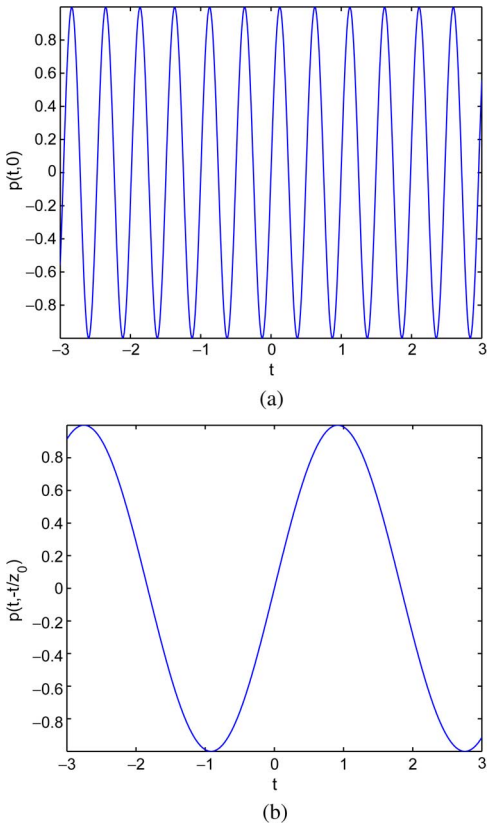

Fig. 8. Slices of the POF of the curved-wall scene along (a) the same pixel line and (b) optical flow line with $z_0 = 11.5$.

pixel line, which confirms the advantage of depth-corrected interpolation in IBR. Using (12) and (32), and the surface depth and slope ranges for the curved-wall scene found in Section VI, we obtain estimates for the maximum frequency for these two slices of the POF as 3.2 and 0.6 Hz, respectively. These estimates closely characterize the function plots in Fig. 8.

VIII. Conclusion

In this paper, we have studied the bandwidth of the POF of a simple scene model where a band-limited signal is painted on a smooth surface. We have shown that, in general, the POF for this model is *not* band limited unless the surface is flat. We then derive a simple rule to estimate the essential bandwidth, defined as the bandwidth where most of the signal energy resides, of the POF for this model. This essential bandwidth is estimated as the product of the bandwidth of the painted signal times the maximum absolute derivative of the surface curvilinear coordinate along a certain direction. Our analysis reveals that, in addition to the maximum and minimum surface depths and the maximum frequency of the painted signal, the bandwidths of the POF also depend on the maximum surface slope. By treating the POF with a unifying formalism based on multidimensional signal processing, we can verify several important results, including induced filtering along the camera dimensions, depth-corrected interpolation in lumigraph, and quantifying the necessary sampling rates. Numerical results show that the resulting estimated bandwidths of the POFs are accurate and effectively characterize the performance of image-based rendering algorithms.

Acknowledgment

The authors would like to thank N. Aggarwal of the University of Illinois at Urbana–Champaign (UIUC), Urbana, for the helpful discussions on the bandwidth of time-warped functions. The late D. Slepian (1923–2007) and his seminal paper [27] have been inspirations for the authors in completing this paper.

References

[1] L. McMillan and G. Bishop, "Plenoptic modeling: An image-based rendering system," in *Proc. SIGGRAPH*, 1995, pp. 39–46.
[2] H.-Y. Shum, S. Kang, and S.-C. Chan, "Survey of image-based representations and compression techniques," *IEEE Trans. Circuits Syst. Video Technol.*, vol. 13, no. 11, pp. 1020–1037, Nov. 2003.
[3] C. Zhang and T. Chen, "A survey on image-based rendering—Representation, sampling and compression," *EURASIP Signal Process.: Image Commun.*, vol. 19, no. 1, pp. 1–28, Jan. 2004.
[4] H.-Y. Shum, S.-C. Chan, and S. B. Kang, *Image-Based Rendering*. New York: Springer-Verlag, 2007.
[5] E. H. Adelson and J. R. Bergen, "The plenoptic function and the elements of early vision," in *Computational Models of Visual Processing*, M. Landy and J. A. Movshon, Eds. Cambridge, MA: MIT Press, 1991, pp. 3–20.
[6] Z. Lin and H.-Y. Shum, "On the number of samples needed in light field rendering with constant-depth assumption," in *Proc. IEEE Conf. Comput. Vis. Pattern Recog.*, 2000, pp. 588–595.
[7] J.-X. Chai, X. Tong, S.-C. Chan, and H.-Y. Shum, "Plenoptic sampling," in *Proc. SIGGRAPH*, 2000, pp. 307–318.
[8] C. Zhang and T. Chen, "Spectral analysis for sampling image-based rendering data," *IEEE Trans. Circuits Syst. Video Technol.*, vol. 13, no. 11, pp. 1038–1050, Nov. 2003.
[9] F. Durand, N. Holzschuch, C. Soler, E. Chan, and F. X. Sillion, "A frequency analysis of light transport," in *Proc. SIGGRAPH*, 2005, pp. 1115–1126.
[10] R. Ng, "Fourier slice photography," in *Proc. SIGGRAPH*, 2005, pp. 735–744.
[11] A. Veeraraghavan, R. Raskar, A. Agrawal, A. Mohan, and J. Tumblin, "Dappled photography: Mask enhanced cameras for heterodyned light fields and coded aperture refocusing," in *Proc. SIGGRAPH*, 2007, pp. 1–14.
[12] M. N. Do, D. Marchand-Maillet, and M. Vetterli, "On the bandlimitedness of the plenoptic function," in *Proc. IEEE Int. Conf. Image Process.*, Genova, Italy, Sep. 2005, pp. III-17–III-20.
[13] M. Levoy and P. Hanrahan, "Light field rendering," in *Proc. SIGGRAPH*, 1996, pp. 31–40.
[14] S. Gortler, R. Grzeszczuk, R. Szeliski, and M. Cohen, "The lumigraph," in *Proc. SIGGRAPH*, 1996, pp. 43–54.
[15] O. D. Faugeras, *Three-Dimensional Computer Vision: A Geometric Viewpoint*. Cambridge, MA: MIT Press, 1993.
[16] R. C. Bolles, H. H. Baker, and D. H. Marimont, "Epipolar-plane image analysis: An approach to determining structure from motion," *Int. J. Comput. Vis.*, vol. 1, no. 7, pp. 7–55, 1987.
[17] D. A. Forsyth and J. Ponce, *Computer Vision: A Modern Approach*. Englewood Cliffs, NJ: Prentice-Hall, 2002.
[18] H. T. Nguyen and M. N. Do, "Error analysis for image-based rendering with depth information," *IEEE Trans. Image Process.*, vol. 18, no. 4, pp. 703–716, Apr. 2009.
[19] G. Miller, S. Rubin, and D. Ponceleon, "Lazy decompression of surface light fields for precomputed global illumination," in *Proc. Eurograph. Rendering Workshop*, Vienna, Austria, 1998, pp. 281–292.
[20] T. Ajdler, L. Sbaiz, and M. Vetterli, "The plenacoustic function and its sampling," *IEEE Trans. Signal Process.*, vol. 54, no. 10, pp. 3790–3804, Oct. 2006.
[21] D. Cochran and J. J. Clark, "On the sampling and reconstruction of time warped band-limited signals," in *Proc. IEEE Int. Conf. Acoust., Speech, Signal Process.*, Apr. 1990, pp. 1539–1541.
[22] X.-G. Xia and Z. Zhang, "On a conjecture on time-warped band-limited signals," *IEEE Trans. Signal Process.*, vol. 40, no. 1, pp. 252–254, Jan. 1992.
[23] S. Azizi, D. Cochran, and J. N. McDonald, "On the preservation of bandlimitedness under non-affine time warping," in *Proc. Int. Workshop Sampling Theory Appl.*, Aug. 1999.
[24] D. Marchand-Maillet, "Sampling theory for image-based rendering," M.S. thesis, Swiss Federal Inst. Technol., Lausanne, Switzerland, 2001.

[25] B. P. Lathi, *Modern Digital and Analog Communication Systems*, 3rd ed. Oxford, U.K.: Oxford Univ. Press, 1998.
[26] G. Wolberg, *Digital Image Warping*. Los Alamitos, CA: IEEE Comput. Soc. Press, 1994.
[27] D. Slepian, "On bandwidth," *Proc. IEEE*, vol. 64, no. 3, pp. 292–300, Mar. 1976.

Minh N. Do (M'01–SM'07) was born in Vietnam in 1974. He received the B.Eng. degree in computer engineering from the University of Canberra, Bruce, ACT, Australia, in 1997 and the Dr.Sci. degree in communication systems from Swiss Federal Institute of Technology Lausanne (EPFL), Lausanne, Switzerland, in 2001.

Since 2002, he has been with the faculty of the University of Illinois at Urbana–Champaign (UIUC), Urbana, where he is currently an Associate Professor with the Department of Electrical and Computer Engineering and holds joint appointments with the Coordinated Science Laboratory, Beckman Institute for Advanced Science and Technology, and the Department of Bioengineering. His research interests include image and multidimensional signal processing, wavelets and multiscale geometric analysis, computational imaging, augmented reality, and visual information representation.

Dr. Do is a member of the IEEE Signal Processing Theory and Methods and Image, Video, and Multidimensional Signal Processing Technical Committees, and an Associate Editor of the IEEE TRANSACTIONS ON IMAGE PROCESSING. He was the recipient of a Silver Medal from the 32nd International Mathematical Olympiad in 1991, a University Medal from the University of Canberra in 1997, a Doctorate Award from the EPFL in 2001, a CAREER Award from the National Science Foundation in 2003, and a Young Author Best Paper Award from IEEE in 2008. He was named a Beckman Fellow at the Center for Advanced Study, UIUC, in 2006 and received the Xerox Award for Faculty Research from the College of Engineering, UIUC, in 2007.

Davy Marchand-Maillet, photograph and biography not available at the time of publication.

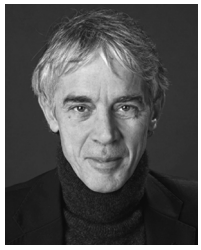

Martin Vetterli (S'86–M'86–SM'90–F'95) received the Dipl. El.-Ing. degree from the Swiss Federal Institute of Technology Zurich (ETHZ), Zurich, Switzerland, in 1981, the M.S. degree from Stanford University, Stanford, CA, in 1982, and the Doctoratès Sciences degree from Swiss Federal Institute of Technology Lausanne (EPFL), Lausanne, Switzerland, in 1986.

He was a Research Assistant with Stanford University and EPFL and with Siemens and AT&T Bell Laboratories. In 1986, he joined Columbia University, New York, where he was an Associate Professor of Electrical Engineering and Co-Director of the Image and Advanced Television Laboratory. In 1993, he joined the University of California, Berkeley, where he was a Professor with the Department of Electrical Engineering and Computer Sciences until 1997, and currently holds an Adjunct Professor position. Since 1995, he has been a Professor of Communication Systems with EPFL, where he Chaired the Communications Systems Division from 1996 to 1997 and currently heads the Audiovisual Communications Laboratory. From 2001 to 2004, he directed the National Competence Center in Research on mobile information and communication systems. He has also been a Vice-President at EPFL since October 2004, in charge, among others, of international affairs and computing services. He held visiting positions at ETHZ and Stanford University in 1990 and 1998, respectively. He was a Plenary Speaker at various conferences (e.g., IEEE ICIP, ICASSP, and ISIT). He is the coauthor of three books, i.e., *Wavelets and Subband Coding* with J. Kovacevic, *Signal Processing for Communications* with P. Prandoni, and *The World of Fourier and Wavelets* with J. Kovacevic and V. K. Goyal. He has published about 140 journal papers on a variety of topics in signal/image processing and communications. He is the holder of a dozen patents. His research interests include sampling, wavelets, multirate signal processing, computational complexity, signal processing for communications, digital image/video processing, joint source/channel coding, signal processing for sensor networks, and inverse problems such as acoustic tomography.

Dr. Vetterli is a Fellow of ACM and EURASIP and a member of SIAM. He was a member of the Swiss Council on Science and Technology from 2000 to 2003. He is with the editorial boards of *Applied and Computational Harmonic Analysis*, the *Journal of Fourier Analysis and Application*, and the IEEE JOURNAL ON SELECTED TOPICS IN SIGNAL PROCESSING. He was the recipient of the Best Paper Award from EURASIP in 1984, the Research Prize from Brown Bovery Corporation (Switzerland) in 1986, the IEEE Signal Processing Society's Senior Paper Awards in 1991, 1996, and 2007 (for papers with D. LeGall, K. Ramchandran, and P. Marziliano and T. Blu, respectively), the Swiss National Latsis Prize in 1996, the SPIE Presidential Award in 1999, and the IEEE Signal Processing Technical Achievement Award in 2001. He is an ISI highly cited researcher in engineering.